NASA TECHNICAL NOTE

NASA TN D-3021

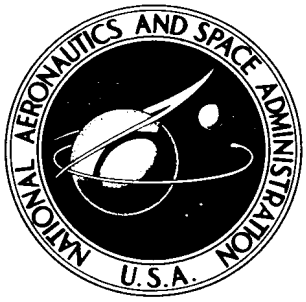

NASA TN D-3021

FLIGHT-DETERMINED LOW-SPEED LIFT AND DRAG CHARACTERISTICS OF THE LIGHTWEIGHT M2-F1 LIFTING BODY

by Victor W. Horton, Richard C. Eldredge, and Richard E. Klein

Flight Research Center
Edwards, Calif.

NATIONAL AERONAUTICS AND SPACE ADMINISTRATION • WASHINGTON, D. C. • SEPTEMBER 1965

NASA TN D-3021

FLIGHT-DETERMINED LOW-SPEED LIFT AND DRAG CHARACTERISTICS OF THE LIGHTWEIGHT M2-F1 LIFTING BODY

By Victor W. Horton, Richard C. Eldredge,
and Richard E. Klein

Flight Research Center
Edwards, Calif.

NATIONAL AERONAUTICS AND SPACE ADMINISTRATION

For sale by the Clearinghouse for Federal Scientific and Technical Information
Springfield, Virginia 22151 – Price $2.00

FLIGHT-DETERMINED LOW-SPEED LIFT AND DRAG CHARACTERISTICS OF THE LIGHTWEIGHT M2-F1 LIFTING BODY

By Victor W. Horton, Richard C. Eldredge,
and Richard E. Klein
Flight Research Center

SUMMARY

The low-speed lift and drag characteristics of a manned, lightweight M-2 lifting-body vehicle were determined in unpowered free-flight tests at angles of attack from 0° to 22° (0.38 radian) and at calibrated airspeeds from 61 knots to 113 knots (31.38 to 58.13 meters/second). Flight data are compared with results from full-scale wind-tunnel tests of the same vehicle.

The investigation showed that 95 percent of the vehicle maximum lift-drag ratio of 2.8 was available through an angle-of-attack range from 4.4° to 14.6° (0.08 to 0.25 radian). Although this lift-drag ratio is considered to be low in comparison with most other aircraft, no serious difficulties were experienced in landing the test vehicle.

The lift and trim characteristics were linear in the angle-of-attack range from 0° to 15° (0.26 radian).

Although the same vehicle was tested in flight and in the wind tunnel, significant differences existed in the values of zero-lift drag and drag due to lift.

INTRODUCTION

In recent years, many wind-tunnel studies have been made during the development of lifting reentry configurations capable of gliding to a specified recovery site and making a conventional horizontal landing. To complement these studies, the NASA Flight Research Center conducted exploratory flight tests of the M-2 lifting-body vehicle.

The M-2 configuration was selected for the flight investigation because of the relatively large amount of aerodynamic data available for the vehicle from previous wind-tunnel studies (refs. 1 to 6). A lightweight version of the M-2 was chosen because of the advantages offered in design simplicity, low cost of construction, simple manual operation of the controls, and ease of maintenance, modification, and repair. This approach also enabled flight

data to be obtained within a relatively short time. A glider-type operation was adopted in preference to on-board propulsion in order to simplify the design and construction of the vehicle and to avoid possible uncertainties in the effects of power on vehicle performance, stability, and control.

This paper presents the low-speed lift and drag characteristics determined in flight for the lightweight M-2 configuration, designated the M2-F1, and compares flight data with full-scale wind-tunnel-test results for the same vehicle. In addition, the rather unusual construction and flight-test techniques used in the program are discussed. The flight tests were conducted at the Flight Research Center, Edwards, Calif., at altitudes below 13,000 feet (3962 meters) and at calibrated airspeeds from 61 knots to 113 knots (31.38 to 58.13 meters/second).

SYMBOLS

Physical quantities used in this paper are given, where applicable, in both the U.S. Customary Units and in the International System of Units (SI). Factors relating the two systems are presented in reference 7.

a_l	longitudinal acceleration, g
a_n	normal-acceleration factor (ratio of the net aerodynamic force along the airplane Z-axis to the weight of the airplane), g
C_D	drag coefficient, $\frac{D}{qS}$
C_{D_b}	base drag coefficient, $\frac{D_b}{qS}$
C_L	lift coefficient, $\frac{L}{qS}$
C_p	pressure coefficient, $\frac{\Delta p}{q_c}$
D	drag force along flight path, pounds (kilograms)
d	distance flown for test, average true speed × time, feet (meters)
g	gravitational acceleration, feet/second^2 (meters/second^2)
Δh	corrected altitude loss, feet (meters)
h'	altitude energy condition, feet (meters)
Δh_p	measured altitude loss, feet (meters)
h_p	pressure altitude, feet (meters)

L	lift force normal to flight path, pounds (kilograms)
L/D	lift-drag ratio
p	test ambient pressure, pounds/foot^2 (newtons/meter^2)
Δp	differential pressure, $p_b - p$, pounds/foot^2 (newtons/meter^2)
p_b	vehicle base pressure, pounds/foot^2 (newtons/meter^2)
q	dynamic pressure, pounds/foot^2 (newtons/meter^2)
q_c	impact pressure, pounds/foot^2 (newtons/meter^2)
S	body area, foot^2 (meter^2)
S_b	base area, foot^2 (meter^2)
t	time, second
V	velocity, feet/second (meters/second)
W	vehicle weight, pounds (kilograms)
α	calibrated angle of attack, degrees (radians)
γ	flight-path angle, degrees (radians)
δ_e	elevon deflection, degrees (radians)
δ_f	flap deflection, degrees (radians)
θ	angle between horizon and horizontal reference plane of vehicle, degrees (radians)

Subscripts:

av	average
b	base
1	initial condition
2	final condition

DESCRIPTION OF TEST VEHICLE

The M2-F1, as shown in figures 1(a) to 1(c) and 2, is a lightweight, single-place glider designed for low-speed exploratory flight studies. Table I presents pertinent physical characteristics of the vehicle. The

"wing" loading W/S was 9 lb/ft^2 (43.9 kg/m^2), and the center of gravity of the vehicle for all flight tests was at approximately 55 percent of the body length. A more detailed description of the vehicle is given in appendix A.

FLIGHT TESTS

A normal flight consisted of a takeoff from Rogers Dry Lake, towed by a C-47 airplane, and a climbing flight path which skirted the edges of the lake to insure that a landing could be made on the lakebed in the event of a tow-line failure. The release altitude ranged from 10,000 feet to 13,000 feet (3048 to 3962 meters) mean sea level, and data were obtained during the subsequent glide to the landing area (2280 feet altitude).

Various maneuvers were performed at speeds ranging from 61 knots to 113 knots calibrated airspeed (KCAS) (31.38 to 58.13 meters/second) and Reynolds numbers from 10.5×10^6 to 19.6×10^6 based on the standard atmosphere at 9000 feet (2743 meters) altitude and the body length of 20 feet (6.1 meters). The last 2000 feet (609.6 meters) of altitude were used by the pilot for the landing maneuver. The flight operations are discussed in detail in appendix A.

WIND-TUNNEL TESTS

Prior to flight, the M2-F1 was tested in the 40- by 80-foot wind tunnel at the Ames Research Center to obtain preliminary performance and control data applicable to the flight program. Tufts were used in these tests to make it possible to see the vortex flow patterns on the upper surface and to identify areas of flow separation. Typical tuft patterns are shown in figures 3(a) and 3(b).

At the conclusion of the flight tests, the vehicle was again placed in the 40- by 80-foot tunnel for a more comprehensive evaluation of the longitudinal characteristics. For this series of tests, the wind-tunnel and flight configurations were nearly identical. The method of mounting the vehicle in the tunnel is shown in figure 4. The tests were performed at tunnel-calibrated airspeeds from 64 knots to 130 knots (32.92 to 66.88 meters/second), Reynolds numbers from 13.8×10^6 to 27.2×10^6 based on standard atmospheric conditions at sea level and the body length of 20 feet (6.1 meters), and angles of attack from -8° to 20° (-0.14 to 0.35 radian).

INSTRUMENTATION

The test vehicle contained standard NACA recording instruments and a synchronizing timer for correlating all quantities pertinent to the lift and drag analysis.

A standard NACA nose boom (ref. 8) provided total and static pressures from positions 51.5 inches (1.3 meters) and 42.5 inches (1.1 meters), respectively, forward of the fuselage zero-reference station. Angle of attack was measured by a vane located about 27.25 inches (0.7 meter) ahead of the reference station.

Special instrumentation consisted of an NACA recording inclinometer, a 12-cell manometer for measuring base pressures, and a static bomb to provide an accurate static source for determination of the base pressures.

Special Calibrations

Since performance data are directly dependent on both angle of attack and airspeed, special calibrations were made to insure accuracy and reliability. The angle-of-attack vane, referenced to the top of the M2-F1 forward body surface which is parallel to the horizontal reference plane, was calibrated during level, unaccelerated airplane-towed flight. The calibration was restricted to a range from 1° to 10° (0.02 to 0.17 radian) by the minimum tow-plane speed at the higher angles and at the lower angles by the towed structural-speed limitation of the M2-F1. Scatter in the data indicated an overall accuracy of about ±1.0° (±0.02 radian).

Data from the flight calibration (fig. 5) agreed with a calibration obtained in the full-scale wind-tunnel tests which covered a considerably larger angle-of-attack range, -7° to 22° (-0.12 to 0.38 radian). The calibration is discussed further in appendix B.

The airspeed system was calibrated during airborne car tows over a measured speed course, during airplane tows with the aid of a calibrated pacer airplane, and in the wind tunnel. Data from the three calibrations, which are discussed in appendix B, agreed as shown in figure 6. Scatter in the data indicated an accuracy of ±1 knot (±0.51 meter/second).

LIFT AND DRAG DETERMINATION

Methods

The primary method of obtaining data utilized sensitive accelerometers for determination of the normal and axial forces. The lift and drag were then calculated from the relationships shown in appendix C (page 16). A detailed explanation of this method may be found in reference 9.

The lift-drag ratios determined by the accelerometer method were checked by using two other techniques, the stabilized glide and the rate of sink. The three methods are discussed and sample calculations are presented in appendix C.

Base-Pressure Measurements

Base pressures were obtained in towed flight at three different stabilized airspeeds. Altitude was maintained constant to eliminate lag effects in the pressure system. A static bomb was used to obtain an accurate measurement of static pressure. The bomb was designed on the basis of information given in reference 10 and was attached to the M2-F1 as shown in figure 7. Base-pressure and base-drag coefficients were calculated from the relationship

$$C_p = \frac{\Delta p}{q_c}$$

where $q_c \approx q$ at test velocity, and

$$C_{D_b} = \frac{S_b}{S} C_{p,av}$$

The average pressure coefficient $C_{p,av}$ was obtained from an average of the pressures measured at the various stations shown in figure 8 and presented in table II.

Measurement Errors and Effects

The estimated maximum errors in the principal measurements were as follows:

W, pounds (kilograms)	±20 (±9.1)
a_n, g	±0.0118
a_l, g	±0.0025
q_c, pounds/foot^2 (newtons/meter^2)	±0.56 (±26.8)
α, degrees (radians)	±1 (±0.02)
θ (inclinometer), degrees (radians)	±0.11 (±0.002)
t, seconds	±0.05
Calibrated airspeed, knots (meters/second)	±1 (±0.51)
h_p, feet (meters)	±50 (±15.2)
Air temperature, deg C	±2

The following table shows a breakdown of the probable error in C_L and C_D resulting from the estimated errors in the measured parameters. Because the measurement errors tend to be random, their combined effect is approximated by the root mean square[1] for all parameters. These data are presented for the accelerometer method of analysis for a flight speed of 82 KCAS (42.18 m/sec).

---

[1]Square root of the sum of errors squared.

Parameter	Estimated measurement error	Resultant error in C_L	Resultant error in C_D
W	±20 lb (±9.1 kg)	±0.006	±0.0020
a_n	±0.0118g	±0.005	±0.0007
a_l	±0.0025g	Negligible	±0.0010
q_c	±0.56 lb/ft^2 (±26.8 N/m^2)	±0.009	±0.0034
α	±1° (±0.02 rad)	±0.002	±0.0066
Combined root-mean-square error		±0.012	±0.0078

Data extracted from the faired curves would be expected to be essentially void of random error and, thus, have a greater accuracy than the root-mean-square value.

The calculations of base-pressure coefficients were based on the assumption that the position error in the airspeed system was negligible. The validity of this assumption can be inferred from the dimensions indicated in figure 7 and the design considerations in reference 10. Hence, the principal source of error in the dynamic-pressure measurements was a combined reading and calibration inaccuracy estimated to be ±0.1 lb/ft^2 (±4.78 N/m^2). The 12-cell manometer used in the base-pressure measurements had a reading accuracy of ±0.25 lb/ft^2 (±11.97 N/m^2), approximately 7 percent of the averaged values.

DISCUSSION OF RESULTS

Lift and Trim Characteristics

Flight data were obtained for trimmed angles of attack ranging from about 0° to 22° (0.38 radian). These limits are approximate and were established at the lower angles by a maximum allowable operational speed of 120 KCAS (61.73 m/sec) and at the upper angles by a pitch flap control stop at δ_f = -18.7° (-0.31 radian).

The flap deflections required for trim between these limits are shown in figure 9 as a function of angle of attack and airspeed. Both flight data and data calculated from wind-tunnel results are included. Although the data variations from the two sources are nearly linear and parallel, the flap deflections from flight are generally lower than those from the wind-tunnel tests. Detailed examination of this difference revealed complications, in flight, resulting from flexibility of the control system and uncertainties in elevon control position. The control system, though entirely adequate for flight, was flexible enough to allow the elevon surface deflection to vary with dynamic pressure and angle of attack.

The wind-tunnel data presented in the following sections were obtained with the control surfaces mechanically fixed according to the ratio of flap to elevon deflection shown in figure 10 for a rigid system (zero dynamic pressure). Conversely, the flight data presented are for a flexible control system, which, it is estimated, would allow the elevons to deviate as much as 2° to 5° (0.03 to 0.09 radian) from the settings given in figure 10. In general, the performance of the M2-F1 was found to be unusually sensitive to the manner in which the flap and elevon deflections were combined. The comparisons of the lift and drag characteristics presented herein should, therefore, be considered in the light of qualitatively determined effects of control-system flexibility. The scatter in the flight data indicates errors in the flap control position of generally less than ±1° (±0.02 radian).

The lift curve in figure 11 shows the shallow slope expected of a low-aspect-ratio shape. The slope, 0.0225 per degree (1.29 per radian), agrees closely with the value given in reference 11 for an equivalent flat delta wing having the same length and span as the M2-F1 vehicle, including the elevons. Although the flight data are essentially linear to angles of attack of about 15°, wind-tunnel data shown in the figure have a slightly greater slope at angles of attack greater than 12° (0.21 radian). When both sets of data are extrapolated to zero lift, the agreement for the zero-lift angle of attack is within 0.2° (0.003 radian).

Examination of the trim curve in figure 9 reveals that less (negative) flap deflection is required to trim at a given angle of attack in flight than in the wind-tunnel tests. Although the data of figure 10 would indicate less negative elevon deflections in flight than in the wind-tunnel tests, the opposite appears to occur in free flight as a result of the flexibility of the elevon control system. This point is supported by qualitative observations of a separate series of wind-tunnel tests in which only the elevon system was allowed to deflect as in flight (i.e., figure 10 does not describe the free-flight flap-elevon relationship).

Drag Characteristics

The drag polars from flight and wind-tunnel tests are presented in figure 12. The difference between the two polars is believed to be the result of two factors: First, the wind-tunnel data show a higher minimum drag, probably caused by interference from the tunnel support system, and, secondly, the flight data show a higher drag due to lift. The latter difference is evident in the linearized polar form shown in figure 13 and, apparently, is largely a result of the greater slope of the wind-tunnel lift curve above $\alpha = 12°$ (0.21 radian) (fig. 11). The wind-tunnel drag coefficients are higher at all measured angles of attack. Included in figure 13 is an estimate of the minimum drag coefficient (see following table) based on the methods of Hoerner (ref. 12).

Base-pressure data were available for both the wind-tunnel and the flight tests and were used in determining the contribution of the base drag to the total drag for each type of test, which provides some insight into the

differences mentioned previously. The data, in drag-coefficient form, are presented in the following table, along with a breakdown of the estimated drag:

	Flow conditions	ΔC_D		
		Estimated (ref. 12)	Flight (a)	Wind tunnel (a)
Skin friction	Turbulent boundary layer	0.0119	---	---
Landing gear	Subcritical Reynolds number	0.0242	---	---
Base drag	Turbulent boundary layer	0.0228	0.0171 0.0205	0.0130 0.0157
Holes (landing gear)	Not applicable	0.0002	---	---
Elevon gaps	Not applicable	0.0006	---	---
Rudder and flap gaps	Not applicable	0.0003	---	---
Elevon base	Two-dimensional	0.0089	[b]0.0025 0.0028	---
Rudder base	Two-dimensional	0.0076	0.0021 0.0024	---
Base of skids	Turbulent	0.0003	[c]0.000019 0.000023	[c]0.000014 0.000018
Fin interference	30 percent of skin friction	0.0036	---	---
Canopy	Turbulent	0.0011	---	---
Total (assumed zero lift)		0.0815	---	---
Total zero-lift from measurements[d] . . .		------	0.0815	0.102

[a]From pressure data, given at low and high angle of attack.
[b]Elevon base pressure assumed same as rudder base pressure.
[c]Skid base pressure assumed same as body base pressure.
[d]Extrapolated to zero-lift in figure 13.

It can be seen that the estimated base drag approximates the flight-derived value at high angle of attack, but both are slightly higher than the wind-tunnel values. Thus, the base drag does not account for the differences between flight and wind-tunnel drag data. It is significant that the sum of body and surface base drag accounts for approximately 22 percent of the total drag near zero angle of attack.

The table shows the fortuity of the drag estimate, inasmuch as all the comparable component test values differ significantly from the estimates.

Lift-Drag Ratio

The results from the three methods used in determining the lift-drag ratio are shown in figure 15 as a function of angle of attack. Ninety-five percent of the maximum lift-drag ratio of 2.8 is available over an angle-of-attack range from 4.4° to 14.6° (0.08 to 0.25 radian). The data obtained by the accelerometer method agree well with, and are confirmed by, the stabilized-glide and rate-of-sink data.

The maximum lift-drag ratio obtained from flight was about 10 percent higher than that obtained from the wind-tunnel tests. In view of the exceptionally low level of the lift-drag ratio for this type of vehicle, a 10-percent difference is considered to be significant and suggests a need in future mission applications for an early flight confirmation of performance predictions based on wind-tunnel data.

No serious problems were encountered in landing the test vehicle at the maximum lift-drag ratio of 2.8.

CONCLUSIONS

The principal results from a low-speed flight-performance investigation of the lightweight, unpowered M2-F1 lifting-body vehicle were as follows:

1. The maximum lift-drag ratio of the vehicle was determined to be 2.8.

2. The lift and trim characteristics were linear in the angle-of-attack range from 0° to 15° (0.26 radian).

3. Ninety-five percent of the maximum lift-drag ratio was available through the angle-of-attack range of 4.4° to 14.6° (0.08 to 0.25 radian).

4. Although the same vehicle was tested in flight and in the wind tunnel, at approximately the same velocities and Reynolds numbers, significant differences existed in the values of zero-lift drag and drag due to lift.

5. No serious difficulties were encountered in landing the vehicle.

Flight Research Center,
National Aeronautics and Space Administration,
Edwards, Calif., July 9, 1965

APPENDIX A

DESCRIPTION OF THE M2-F1 VEHICLE AND FLIGHT OPERATIONS

M2-F1

Hull and internal structure.— The M2-F1 is comprised of two major assemblies: the hull, which includes the cockpit and control surfaces, and the internal structure. The hull assembly is constructed of 3/32-inch (2.38 mm) mahogany plywood skin and 1/8-inch (3.18 mm) mahogany rib sections reinforced with spruce. The exterior surface is wrapped with Dacron and doped to provide a more durable finish. The vertical fins, rudders, and elevons are thick slab sections constructed with 0.016-inch (0.41 mm) aluminum skin. The trailing-edge flaps are composed of welded 0.028-inch (0.71 mm) aluminum tubing covered with Dacron and are equipped with fixed trim tabs to reduce the stick forces to a comfortable level. Turning vanes were attached to the side of the hull (for flight and wind-tunnel tests) to alleviate the flap "buzz" in the 95-knot to 105-knot (48.87 to 54.02 meters/second) speed range, which was a result, apparently, of the vortex pattern shed from the vehicle base. A modified glider canopy of molded Plexiglas and plywood encloses the cockpit and access hole that was provided for removal of the internal structure. A Plexiglas nose and side window are also included to provide additional visibility during landing. Styrofoam tail skids were placed on the hull to prevent damage in the event of overrotation in landing or takeoff.

The internal structure (fig. 16), which is constructed of welded steel tubing, includes the fixed landing-gear assembly, control stick, rudder pedals, and control system from the cockpit to a mixer plate. The nosewheel and main-wheel assemblies are slightly modified light-aircraft types, and the main-gear shock and strut assembly incorporates both a viscous damper and a bungee. The seat is a modified rocket ejection seat. Differential main-wheel braking and a steerable nosewheel are provided for ground control.

Control system.— The control system is conventional. Gearing ratios were initially determined with the aid of a ground-based simulation of the vehicle response characteristics, then adjusted to be conventional with flight experiences of the pilot (ref. 13). The longitudinal-control system consists of both a trailing-edge flap and elevons. For pitch control, the elevons are deflected approximately 2.2 times the flap deflection, as shown in figure 10. This ratio results in the elevons maintaining a nearly constant 10° (0.17 radian) local angle of attack at all trimmed conditions ($\alpha_{local} \approx 1.7\alpha + \delta_e$). Roll control is obtained through differential deflection of the elevons, and directional control is provided by the rudders. The longitudinal forces are reduced from an estimated 25 pounds to 30 pounds (13.34 to 13.61 kilograms) pull force to about 5 pounds to 10 pounds (2.27 to 4.54 kilograms) by means of fixed tabs on the flaps. The rudder and elevon forces are very light and require the use of bungees to provide the desired "feel."

Landing-assist rocket.— Because of the anticipated low lift-drag ratio and poor visibility from the cockpit of the M2-F1 during the flare portion of the landing, some means was deemed necessary to provide the pilot with extra time for maneuvering in the event of a difficult landing. A simple and efficient means for increasing the flare time was to equip the vehicle with a small solid-propellant rocket motor with the thrust vector alined longitudinally through the center of gravity. The rocket, when fired, effectively increases the maximum lift-drag ratio from 2.8 to 4.5. The rocket, a small solid-propellant type developed by the Naval Ordnance Test Station at China Lake, Calif., was installed in the base of the M2-F1. It provided a nominal thrust of 180 pounds (801 newtons) for approximately 11 seconds.

Flight Operations

The flight program for the M2-F1 began with a series of taxi tests on car tow to check out the control rigging and to familiarize the pilot with the ground stability of the vehicle. As the pilot acquired confidence and experience, tow speeds were gradually increased (lift-off was achieved at about 75 KCAS (38.58 m/sec)), until a maximum of about 105 KCAS (54.02 m/sec) was reached, which corresponded to 87 percent of the design limit speed. About 60 airborne car tows were completed before the first airplane tow was made.

The light wing loading and unknown control and stability of the test vehicle presented a possible problem, in that the pilot could lose control of the vehicle if the turbulence in the wake of the tow plane were encountered. To determine an acceptable range of tow positions and to assess the effects of takeoff acceleration, several trial tows were made using a conventional sailplane. The results of these tests indicated that a high tow position, about 150 feet (45.7 meters) above the C-47 airplane, and a towline length of about 1000 feet (304.8 meters) would minimize the wake effects of the tow airplane.

Also, before the first airplane tow, four rocket firings were made with the M2-F1 to demonstrate the structural integrity of the rocket installation and to discover any possible adverse thrust effects on the stability and control of the vehicle. Two of the firings were made with the vehicle in motion. The first test, during a car tow at about 60 KCAS (30.87 m/sec) with only the nosewheel off the ground, revealed no noticeable pitch or yaw perturbations. The second firing, also during a car tow, was made while the vehicle was airborne at an altitude of approximately 10 feet (3.05 meters) and a speed of 95 KCAS (48.87 m/sec) after towline release. In this instance, the pilot believed the vehicle stability to be slightly improved while the rocket was burning.

Although available to the pilots on all flights, the landing-assist rocket was used only twice during the program of 37 flights. In one instance, the rocket was used as a precautionary measure when turbulence was encountered during the flare portion of the flight. In the other, the pilot felt that he had leveled off too high and used the rocket to insure a low vertical velocity at touchdown. In both cases, the pilot made a normal landing and reported

that the rocket was beneficial in increasing the apparent lift-drag ratio and the lateral-directional stability.

All air-tow tests were made in the early morning to take advantage of the normally calm air. Initially, the flights were postponed if steady surface winds exceeded 5 knots (2.57 meters/second). As the pilot acquired more experience, this requirement was relaxed until flights were made in steady, 10-knot to 15-knot (5.14 to 7.22 meters/second) winds with light turbulence.

APPENDIX B

SPECIAL CALIBRATIONS

It was impractical to position the airspeed head far enough in front of the vehicle body to eliminate flow-interference effects on the static-pressure source and angle-of-attack vane. Detailed calibrations of the angle-of-attack and airspeed systems were, therefore, required.

Angle-of-Attack Calibration

Angle of attack was measured by a small vane attached to the nose boom and was calibrated during level, unaccelerated airplane-towed flight. The vane readings were compared with those from the longitudinal accelerometer and the recording inclinometer. This technique makes use of the relationship $\theta = \gamma + \alpha$, which, for the assumed flight conditions, reduces to $\gamma = 0°$ and $\theta = \alpha$. Both instruments were alined within 1 minute of arc (0.00029 radian) with the top surface of the vehicle, which was used as a reference for angle of attack. The inclinometer, therefore, recorded angle of attack directly; whereas, the accelerometer readout was related to angle of attack by means of the expression $\theta = \alpha = \sin^{-1}a_z$. Results from both the flight and wind-tunnel calibrations are shown in figure 5. The entire angle-of-attack range available for flight could not be calibrated in flight because of minimum tow-plane speed at the higher angles and the M2-F1 towed structural speed at the lower angles. The wind-tunnel tests, on the other hand, covered a large angle-of-attack range and agreed well with the flight calibration.

Airspeed Calibration

During the wind-tunnel tests, airspeed data were obtained corresponding to four trimmed angles of attack in flight. These points, shown as squares in the calibration presented in figure 6, lie essentially along a straight line. Flight calibration points were obtained by ground towing at the lower speeds and by air towing beside a pacer airplane at the higher speeds.

A 2.5-statute-mile (4023.4 meters) course on Rogers Dry Lake was used for the ground tows over which the stabilized indicated airspeed and elapsed time were recorded for traverses in both directions in order to compensate for any wind effects. By taking into account the test altitude, ambient temperature, and average ground speed, the calibrated airspeed was determined. The corresponding indicated airspeed was corrected for instrument error, which was obtained from a laboratory calibration of the instrument. Calibration data obtained by this method (triangular symbols in fig. 6) were limited by the minimum safe lift-off speed of the M2-F1 and the maximum speed obtainable by the tow car.

The pacer calibration was obtained during airplane tow by taking data points simultaneously from the M2-F1 and the pacer airplane, after both were stabilized in formation, at a series of indicated airspeeds. The calibration data, using this method, were limited by the same factors as the angle-of-attack calibration.

The calibrations obtained by these three techniques showed excellent agreement.

APPENDIX C

THREE METHODS OF LIFT AND DRAG DETERMINATION

Accelerometer Method

The accelerometer method was the primary means used to obtain the data presented in this paper. This method relies on measurements of the normal and axial accelerations and angle of attack. The lift and drag are then calculated from the following relationships

$$L = (a_n \cos \alpha + a_l \sin \alpha) \frac{W}{g}$$

$$D = (a_l \cos \alpha - a_n \sin \alpha) \frac{W}{g}$$

$$C_L = \frac{L}{qS}$$

$$C_D = \frac{D}{qS}$$

$$\frac{L}{D} = \frac{C_L}{C_D} = \frac{a_n \cos \alpha + a_l \sin \alpha}{a_n \sin \alpha - a_l \cos \alpha}$$

The following measured parameters and computations are representative of this method for flight at 82 KCAS (42.18 m/sec)

α, deg (rad)	9.1 (0.16)
a_n, g	1.017
a_l, g	-0.190

$$\frac{L}{D} = \frac{C_L}{C_D} = \frac{a_n \cos \alpha + a_l \sin \alpha}{a_n \sin \alpha - a_l \cos \alpha}$$

$$\frac{L}{D} = \frac{1.017(0.9874) + (-0.190)(0.15816)}{1.017(0.15816) - (-0.190)(0.9874)}$$

$$= 2.80$$

This method has the particular advantage of enabling many data points to be obtained during a single flight. Thus, by performing a gentle pushover to the maximum airspeed and a gradual pullup to the minimum speed, the entire lift-drag curve may be obtained in one continuous maneuver.

Stabilized-Glide Method

The second method--stabilized glide--is based on the following relationship for a stabilized glide (constant indicated airspeed)

$$\frac{L}{D} = -\cot \gamma$$

in which $\gamma = \theta - \alpha$. In the M2-F1 tests, the attitude angle θ was obtained from either the recording inclinometer or the longitudinal accelerometer. The inclinometer recorded θ directly during the stabilized glides, whereas the indicated longitudinal acceleration was equal to $\sin \theta$. This method is the simplest and most direct means of obtaining the lift-drag ratio, but it is also the most difficult to apply because of the requirement for highly stabilized flight conditions at the different angles of attack.

An example of the data reduction for this method is as follows for flight at 82 KCAS (42.18 m/sec)

α, deg (rad)	9.1 (0.16)
a_l, g	-0.190

For a stabilized glide $\sin \theta = a_l$, giving $\theta = -10.95°$ (-0.19 radian). The lift-drag ratio is then obtained from the equation

$$\frac{L}{D} = \cot(\theta - \alpha)$$

$$= \cot(-10.95 - 9.10)$$

$$= \cot(-20.05)$$

$$= 2.74$$

Rate-of-Sink Method

The third method is the rate-of-sink technique, often used by glider pilots to determine the ratio of lift to drag. This method is based on an entirely different set of parameters than the two previous methods. Instead of angles and accelerations, the method relies on measurements of airspeed, altitude, temperature, and time. These parameters, with appropriate corrections, are used to determine the lengths of the sides of a right triangle, which, in turn, determines the glide ratio for a given airspeed or angle of attack:

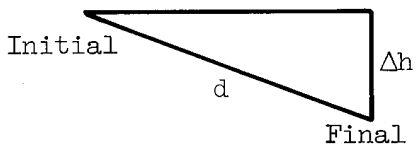

The third side is then equal to $\sqrt{d^2 - \Delta h^2}$, and the glide ratio or L/D is given by the equation

$$\frac{L}{D} = \frac{\sqrt{d^2 - \Delta h^2}}{\Delta h}$$

Data reduction for the one data point obtained by this method is as follows:

	Initial condition	Final condition
t, second	0	52.85
h_p, feet (meters)	8855 (2699)	3905 (1190)
Indicated airspeed, knots (meters/second)	110 (56.59)	110 (56.59)
Calibrated airspeed, knots (meters/second)	113 (58.13)	113 (58.13)
Ambient air temperature, deg C	0.5	2

To determine the distance the aircraft traveled during the 52.85-second test period, the average indicated airspeed, as determined by the pilot, was corrected for the air-data position error. Using an average test temperature of 1.3° C, an average true speed of 123.1 knots (63.33 meters/second) or 207.8 ft/sec (63.34 m/sec) was then calculated. The distance flown was, then,

$$d = (\text{average true airspeed} \times \text{time})$$

$$= 10{,}990 \text{ feet } (3350 \text{ meters})$$

The initial and final true airspeeds were found to be 127.5 knots (65.59 meters/second) or 215.2 ft/sec (65.59 m/sec) and 118.6 knots (61.01 meters/second) or 200.1 ft/sec (60.99 m/sec), respectively, based on the ambient temperatures at these conditions.

To obtain the altitude loss Δh_p for the above time interval, the final pressure altitude $h_{p,2}$ was subtracted from the initial value $h_{p,1}$ and the difference corrected for the deviation from a standard atmosphere as follows

$$\Delta h_p \approx (h_{p,1} - h_{p,2}) \frac{\text{Average test temperature}^1}{\text{Average standard temperature}^1}$$

$$\approx 4930 \text{ feet } (1503 \text{ meters})$$

If there is a difference between the initial and final true airspeeds, a correction must be applied to the altitude loss. A gain in speed corresponds to a gain in kinetic energy which, in turn, means that the aircraft lost more altitude than if it had been maintained at a constant airspeed. The correction must, therefore, be subtracted from the altitude loss. The magnitude

[1] In deg C absolute.

of this correction may be estimated from the interchange between kinetic and potential energy[1] as follows

$$h' = \frac{\left(V_2^2 - V_1^2\right)}{2g}$$

$$= -98 \text{ feet } (-29.9 \text{ meters})$$

Therefore, the corrected altitude loss is

$$\Delta h = \Delta h_p - h'$$

$$= 5028 \text{ feet } (1533 \text{ meters})$$

The corrected distances are then used to obtain the lift-drag ratio as follows

$$\frac{L}{D} = \frac{\sqrt{d^2 - \Delta h^2}}{\Delta h}$$

$$= 1.95$$

To determine the lift-drag ratio by this method with suitable accuracy, the aircraft must be glided at nearly constant indicated airspeed for a relatively long time in order to minimize the effects of measurement inaccuracies, particularly altitude and time. Generally, only one data point per flight can be obtained in this manner.

The rate-of-sink technique is advantageous in that it requires a minimum of instrumentation and, if desired, can rely on the pilot's instruments normally installed in an aircraft.

Estimated Accuracy of Methods

The following tables show a breakdown of the probable error in the L/D data, for each of the three methods, that could result from the estimated measurement errors for the various parameters used. Because the measurement inaccuracies tend to be random, their combined effect on the L/D measurement is given by the root mean square of the sum of the errors for each parameter.

---

[1]This derivation assumes that at the end of the test interval the test aircraft would experience an instantaneous exchange of kinetic and potential energy.

ACCELEROMETER METHOD

[82 KCAS (42.18 m/sec)]

Parameter	Estimated measurement error	Resultant error in L/D
a_n	±0.0118g	±0.02
a_l	±0.0025g	±0.02
α	±1.0° (±0.02 rad)	±0.15
Combined root-mean-square error		±0.15

STABILIZED-GLIDE METHOD

[82 KCAS (42.18 m/sec)]

Parameter	Estimated measurement error	Resultant error in L/D
θ (inclinometer)	±0.15° (±0.003 rad)	±0.03
θ, (a_l)	±0.10° (±0.002 rad)	±0.02
α	±1.0° (±0.02 rad)	±0.16
Combined root-mean-square error		±0.16

RATE-OF-SINK METHOD

[113 KCAS (58.13 m/sec); Δh_p = 4930 ft (1503 m) during 52.9 sec]

Parameter	Estimated measurement error	Resultant error in L/D
t	±0.10 sec	±0.01
Calculated air-speed	±1.0 knot (±0.51 m/sec)	±0.01
Temperature	±2.0° C	±0.01
h_p	±50.0 ft (±15.2 m)	±0.07
Combined root-mean-square error		±0.10

The results from the three methods agree and yield approximately the same root-mean-square deviation, about 5 percent, from the faired curve as shown in figure 15 for the given conditions. As seen in the analyses, which is valid only for vehicles with low lift-drag ratios, the first two methods are highly dependent upon an accurate measurement of angle of attack, whereas the other method is sensitive to the accuracy with which the altitude loss is

measured. Although the accelerometer method does not appear to be the most accurate, its accuracy is ameliorated by the large amount of data that can be gathered on one maneuver. By fairing through a large number of data points, it can be assumed that the resultant data would be essentially void of random error.

REFERENCES

1. Savage, Howard F.; and Tinling, Bruce E.: Subsonic Aerodynamic Characteristics of Several Blunt, Lifting, Atmospheric-Entry Shapes. NASA Memo 12-24-58A, 1959.

2. Dennis, David H.; and Edwards, George G.: The Aerodynamic Characteristics of Some Lifting Bodies. NASA TM X-376, 1960.

3. Kenyon, George C.; and Edwards, George G.: A Preliminary Investigation of Modified Blunt 13° Half-Cone Re-entry Configurations at Subsonic Speeds. NASA TM X-501, 1961.

4. Rakich, John V.: Aerodynamic Performance and Static-Stability Characteristics of a Blunt-Nosed, Boattailed, 13° Half-Cone at Mach Numbers From 0.6 to 5.0. NASA TM X-570, 1961.

5. Kenyon, George C.; and Sutton, Fred B.: The Longitudinal Aerodynamic Characteristics of a Re-entry Configuration Based on a Blunt 13° Half-Cone at Mach Numbers to 0.92. NASA TM X-571, 1961.

6. Axelson, John A.: Pressure Distributions for the M-2 Lifting Entry Vehicle at Mach Numbers of 0.23, 5.2, 7.4 and 10.4. NASA TM X-997, 1964.

7. Mechtly, E. A.: The International System of Units - Physical Constants and Conversion Factors. NASA SP-7012, 1964.

8. Richardson, Norman R.; and Pearson, Albin O.: Wind-Tunnel Calibrations of a Combined Pitot-Static Tube, Vane-Type Flow-Direction Transmitter, and Stagnation-Temperature Element at Mach Numbers From 0.60 to 2.87. NASA TN D-122, 1959.

9. Beeler, De E.; Bellman, Donald R.; and Saltzman, Edwin J.: Flight Techniques for Determining Airplane Drag at High Mach Numbers. NACA TN 3821, 1956.

10. Gracey, William: Measurement of Static Pressure on Aircraft. NACA Rept. 1364, 1958.

11. DeYoung, John; and Harper, Charles W.: Theoretical Symmetric Span Loading at Subsonic Speeds for Wings Having Arbitrary Plan Form. NACA Rept. 921, 1948.

12. Hoerner, Sighard F.: Fluid-Dynamic Drag. Publ. by the author (148 Busteed Drive, Midland Park, N. J.), 1958.

13. Smith, Harriet J.: Evaluation of the Lateral-Directional Stability and Control Characteristics of the Lightweight M2-F1 Lifting Body at Low Speeds. NASA TN D-3022, 1965.

TABLE I

PHYSICAL CHARACTERISTICS OF THE M2-F1

Body –	
Area, foot^2 (meter^2)	139 (12.91)
Span, feet (meters)	9.5 (2.90)
Length, feet (meters)	20 (6.10)
Aspect ratio:	
Basic vehicle	0.65
Including control surfaces	1.23
Weight, including pilot, pounds (kilograms)	1250 (567)
Center of gravity, percentage of reference length	55
Base area, foot^2 (meter^2)	25 (2.32)
Flap –	
Area, foot^2 (meter^2)	17.2 (1.60)
Leading-edge span, feet (meters)	8.7 (2.65)
Trailing-edge span, feet (meters)	6.9 (2.10)
Chord, feet (meters)	2.2 (0.67)
Flap travel, degrees (radians):	
Up	-19.5 (-0.34)
Down	-5 (-0.09)
Elevons (two) –	
Area, each, foot^2 (meter^2)	6.7 (0.62)
Span, feet (meters)	2.4 (0.73)
Root chord, feet (meters)	3.84 (1.17)
Tip chord, feet (meters)	0.83 (0.25)
Aileron travel, degrees (radians)	±14 (±0.24)
Elevator travel, degrees (radians):	
Up	-22 (-0.38)
Down	9 (0.16)
Base area, each, foot^2 (meter^2)	1.13 (0.105)
Vertical stabilizers (two) –	
Area, each, foot^2 (meter^2)	11.6 (1.08)
Height, feet (meters)	3.4 (1.04)
Chord, feet (meters)	5.9 (1.80)
Rudders (two) –	
Area, each, foot^2 (meter^2)	5.3 (0.49)
Height, feet (meters)	4.3 (1.31)
Chord, feet (meters)	1.3 (0.40)
Travel, degrees (radians)	±4.5 (±0.08)
Base area, each, foot^2 (meter^2)	0.95 (0.09)

TABLE II

BASE-PRESSURE COEFFICIENTS

Orifice (a)	q_c = 38.55 lb/ft^2 (1845.8 N/m^2), α = 4.4° (0.08 rad)		q_c = 31.70 lb/ft^2 (1517.8 N/m^2), α = 5.7° (0.10 rad)		q_c = 26.65 lb/ft^2 (1276.0 N/m^2), α = 9.2° (0.16 rad)	
	Δp, lb/ft^2 (N/m^2)	C_p (b)	Δp, lb/ft^2 (N/m^2)	C_p (b)	Δp, lb/ft^2 (N/m^2)	C_p (b)
1	-3.00 (-143.6)	-0.078	-2.00 (-95.8)	-0.063	-2.50 (-119.7)	-0.094
2	-2.25 (-107.7)	-0.058	-2.00 (-95.8)	-0.063	-1.25 (-59.9)	-0.047
3	-3.75 (-179.6)	-0.097	-3.75 (-179.6)	-0.118	-2.50 (-119.7)	-0.094
4	-3.50 (-167.6)	-0.091	-3.00 (-143.6)	-0.095	-3.00 (-143.6)	-0.113
5	-4.75 (-227.4)	-0.123	-4.25 (-203.5)	-0.134	-4.00 (-191.5)	-0.150
6	-4.75 (-227.4)	-0.123	-4.75 (-227.4)	-0.150	-4.75 (-227.4)	-0.178
7	-3.75 (-179.6)	-0.097	-3.25 (-155.6)	-0.103	-3.25 (-155.6)	-0.122
8	-3.25 (-155.6)	-0.084	-2.75 (-131.7)	-0.087	-2.00 (-95.8)	-0.075
9	-3.50 (-167.6)	-0.091	-2.25 (-107.7)	-0.071	-3.00 (-143.6)	-0.113
12	-4.25 (-203.5)	-0.110	-3.75 (-179.6)	-0.118	-4.00 (-191.5)	-0.150
	Average values of orifices 1 to 9 and 12					
	-3.68 (-176.2)	-0.095	-3.18 (-152.3)	-0.100	-3.03 (-145.1)	-0.114
10	-6.25 (-299.3)	-0.162	-5.00 (-239.4)	-0.158	-4.00 (-191.5)	-0.150
11	-5.50 (-263.3)	-0.143	-4.75 (-227.4)	-0.150	-5.25 (-251.4)	-0.197
	Average values of orifices 10 and 11					
	-5.88 (-281.5)	-0.153	-4.88 (-233.7)	-0.154	-4.63 (-221.7)	-0.174

[a]Orifices 1 to 9 and 12 are attached to the body base. Orifices 10 and 11 are attached to the rudder base.

[b]$C_p = \Delta p/q_c$, where q_c is the differential between nose-boom total pressure and static-bomb static pressure.

E-10842

(a) Side view.

Figure 1.- External characteristics of the M2-F1.

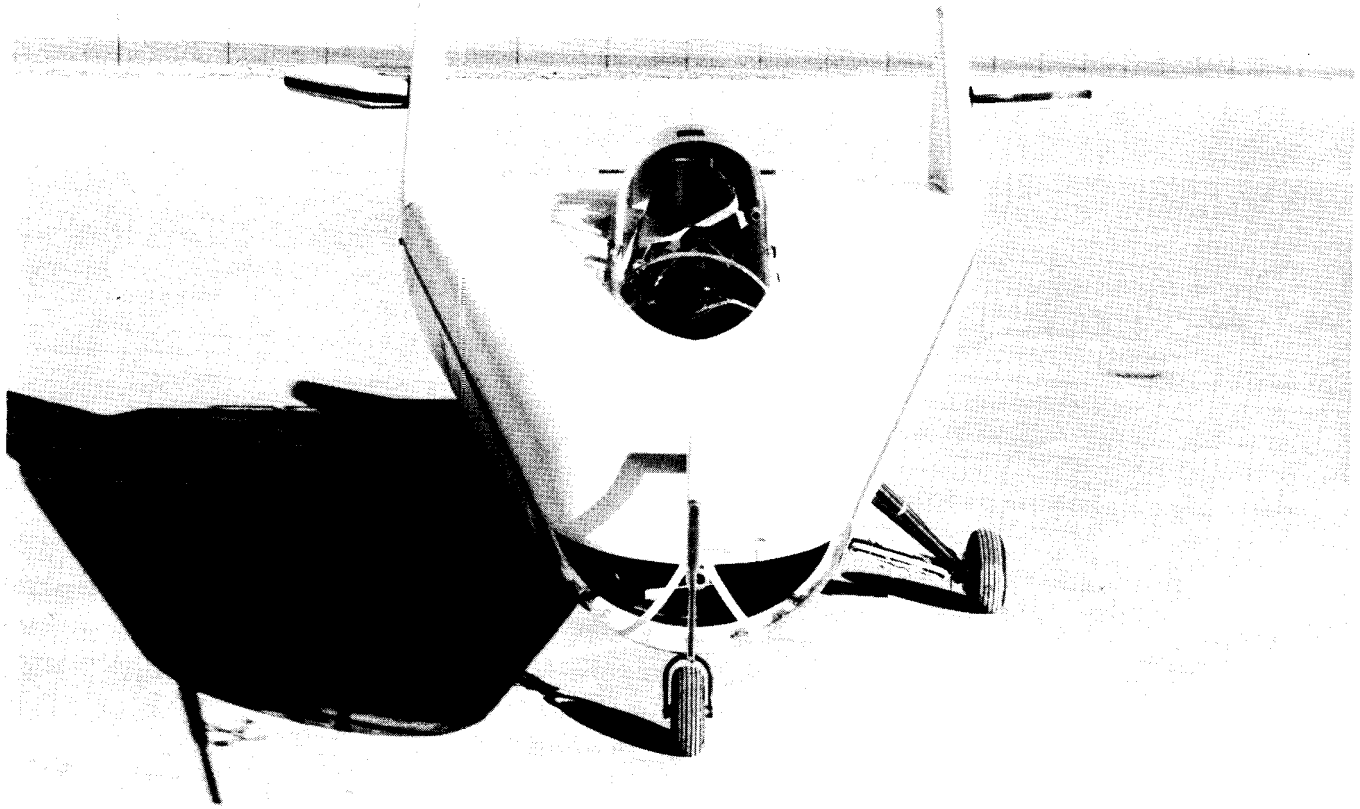

E-10811

(b) Front view.

Figure 1.- Continued.

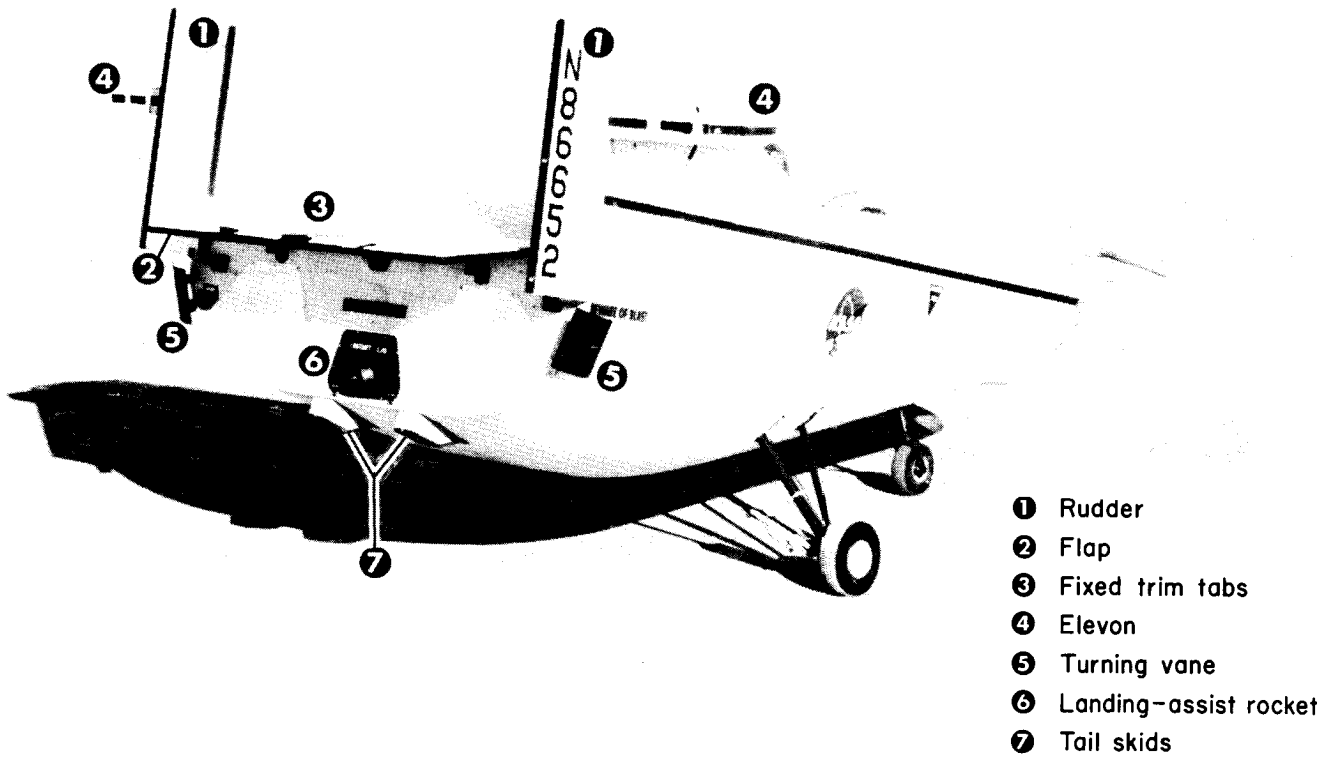

E-13655

(c) Rear three-quarter view.

Figure 1.- Concluded.

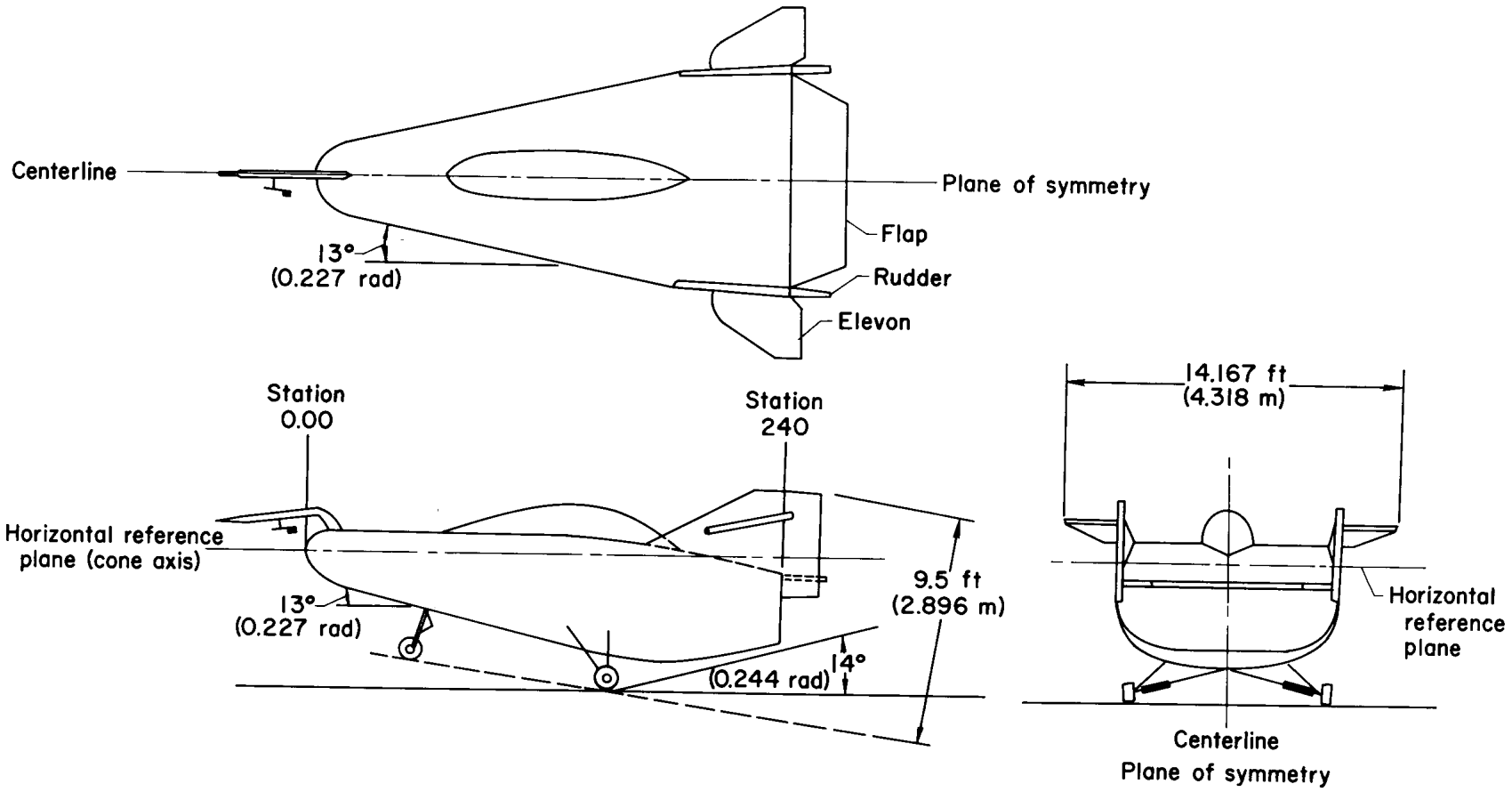

Figure 2.- Three-view drawing of the M2-F1.

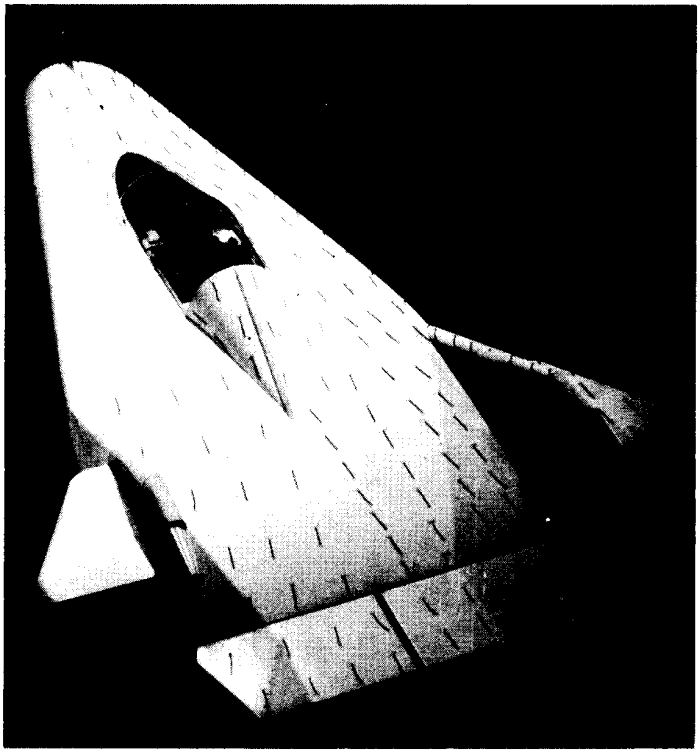

(a) Top view.

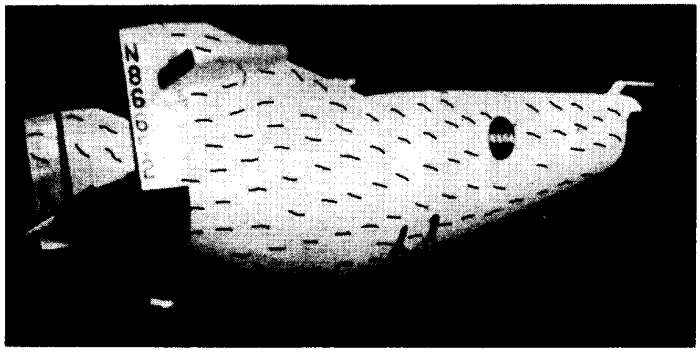

(b) Side view.

Figure 3.– Flow visualization by tufts in the wind tunnel.

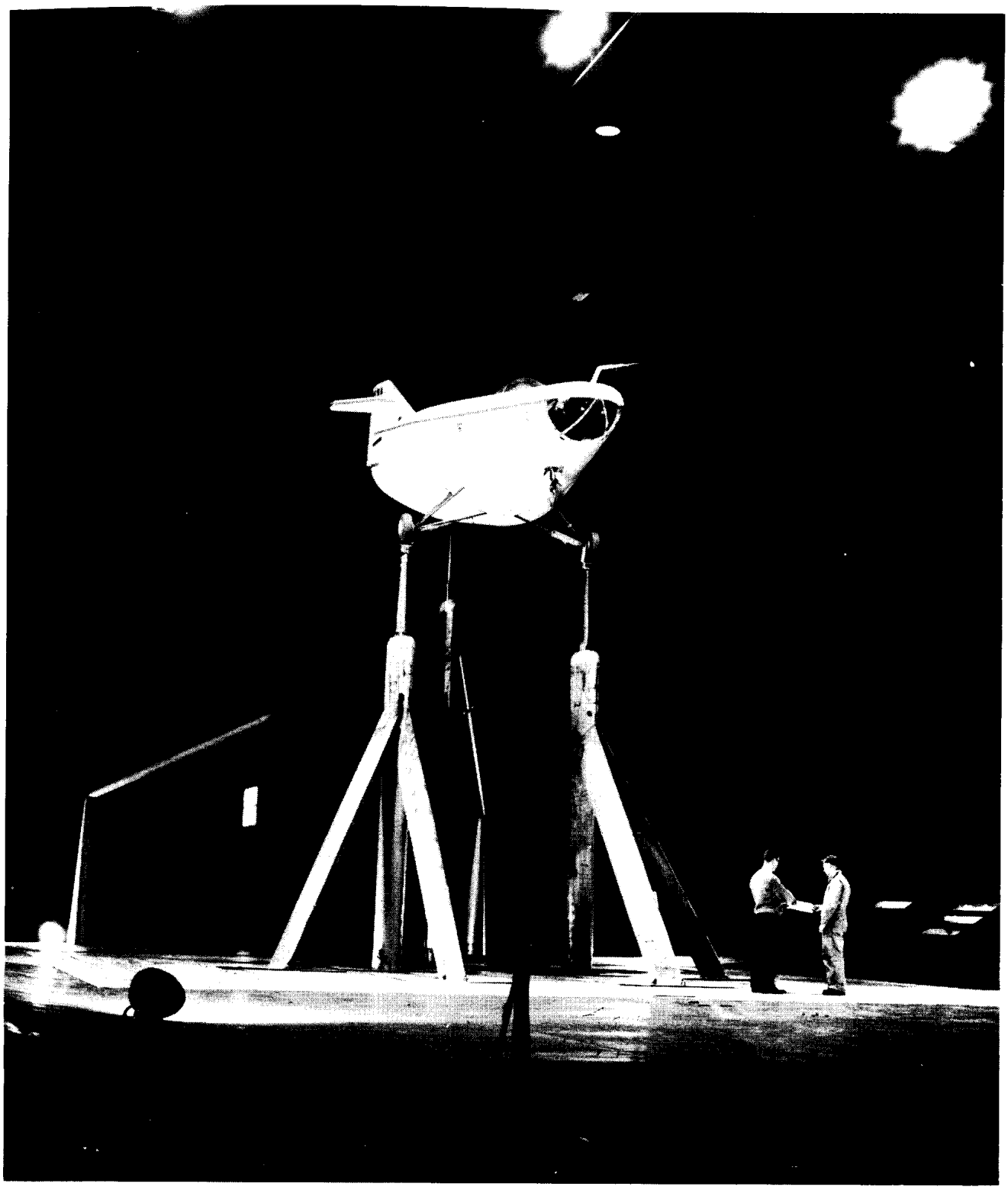

A-33718

Figure 4.— Mounting arrangement in the 40- by 80-foot Ames Research Center wind tunnel.

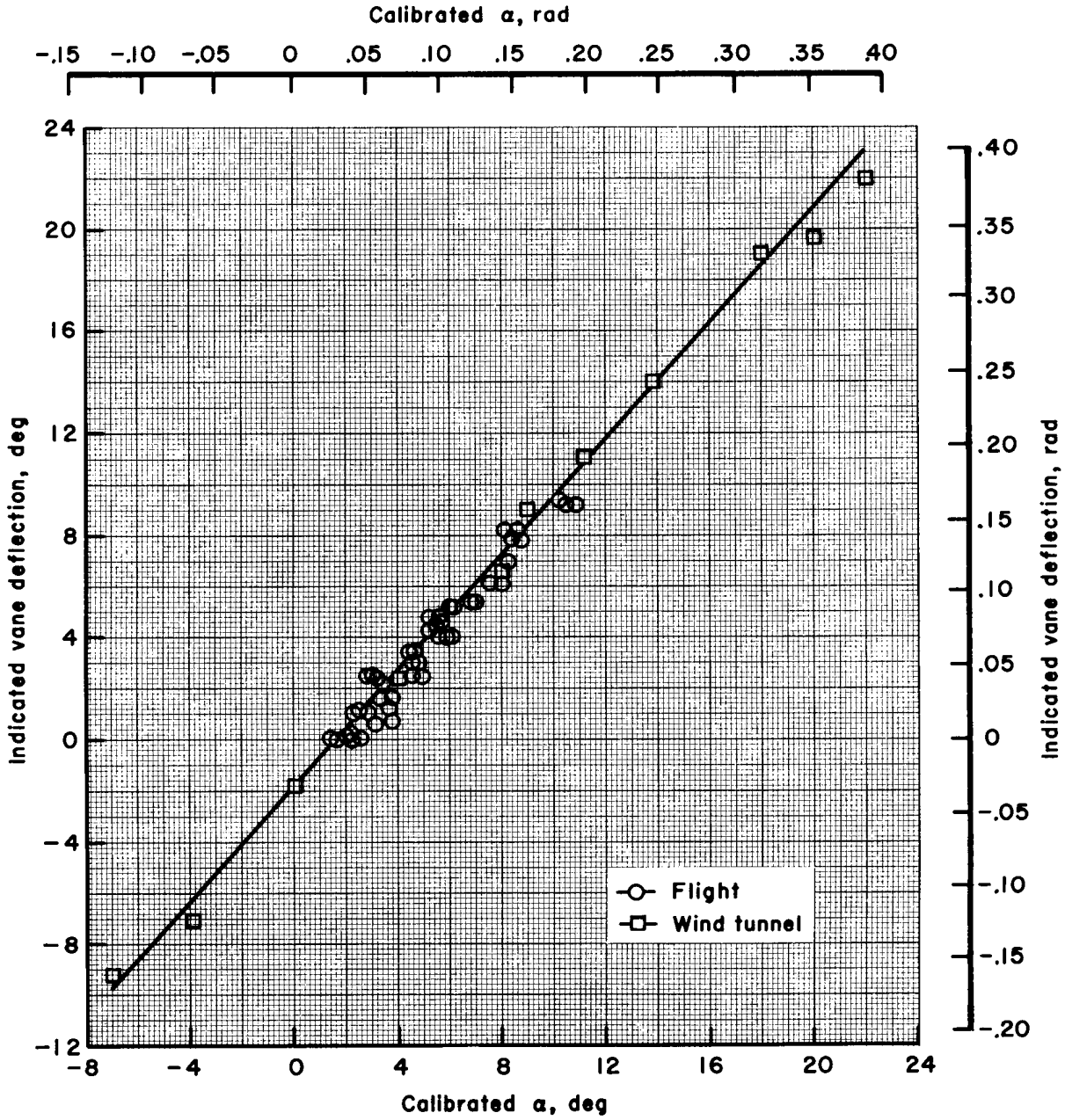

Figure 5.- Angle-of-attack calibration.

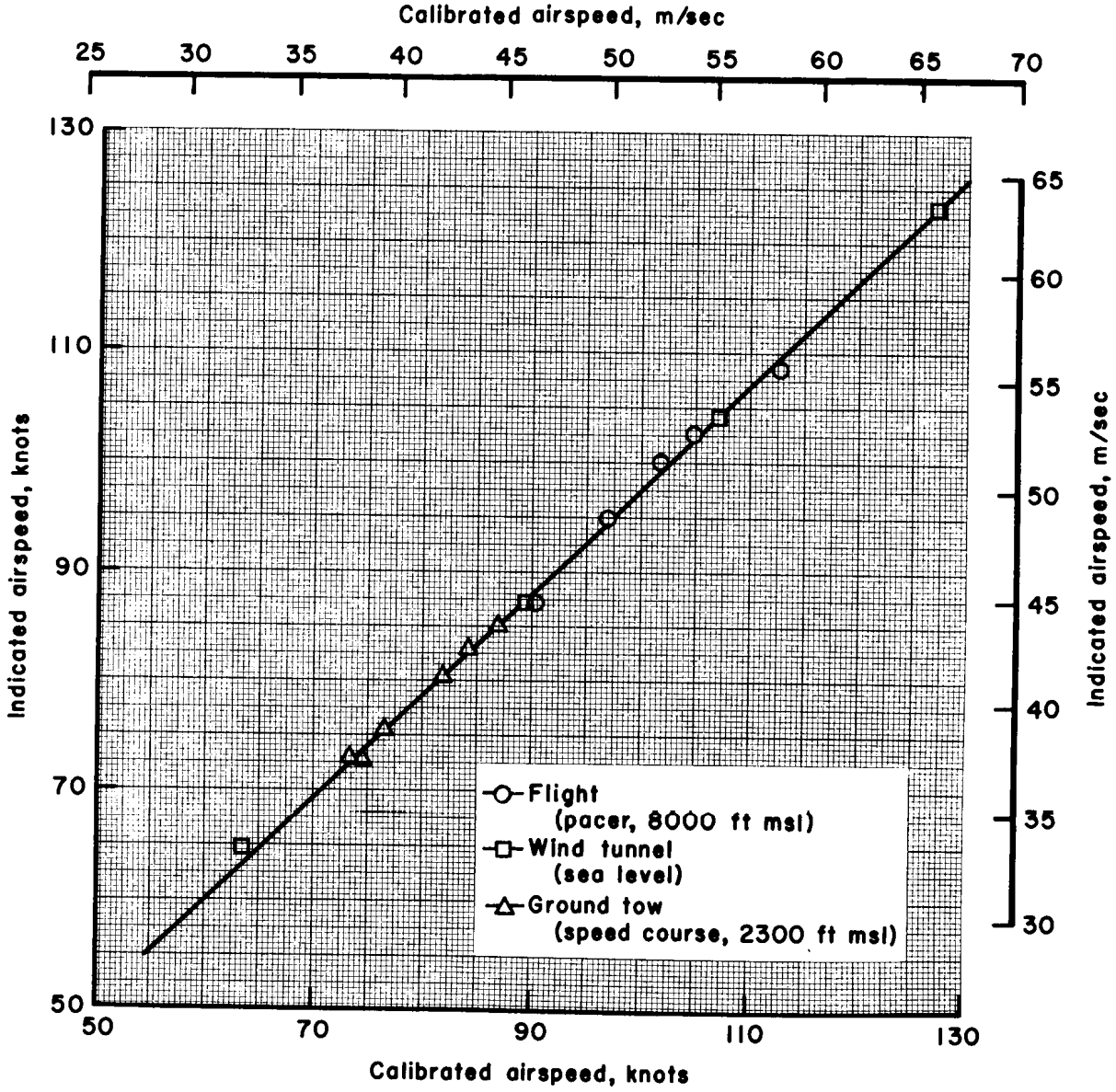

Figure 6.– Airspeed calibration.

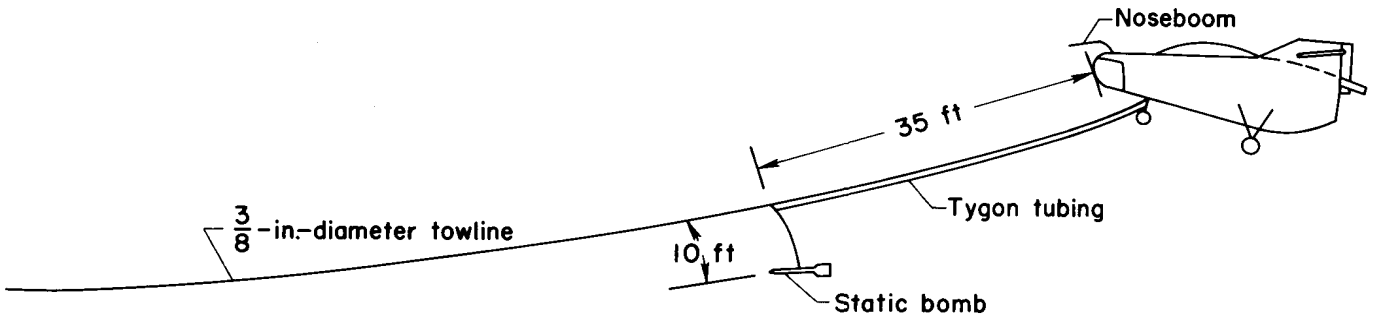

(a) Static-bomb attachment.

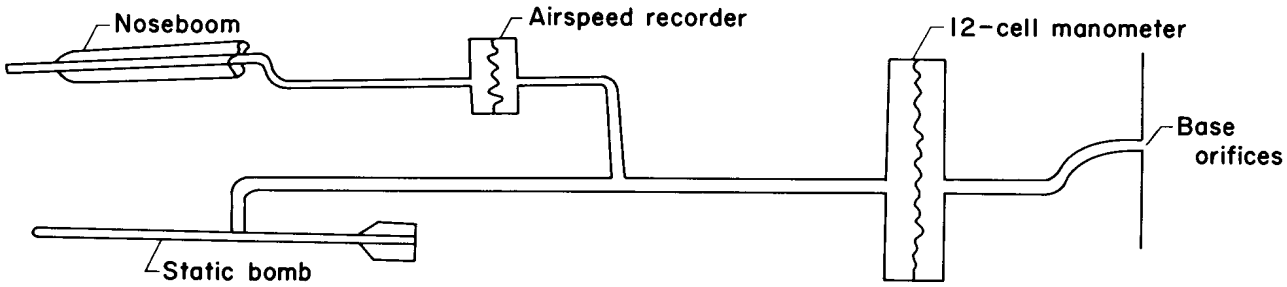

(b) Schematic of base-pressure-measuring system.

Figure 7.– Arrangements for obtaining static pressure during tow for base-pressure measurements.

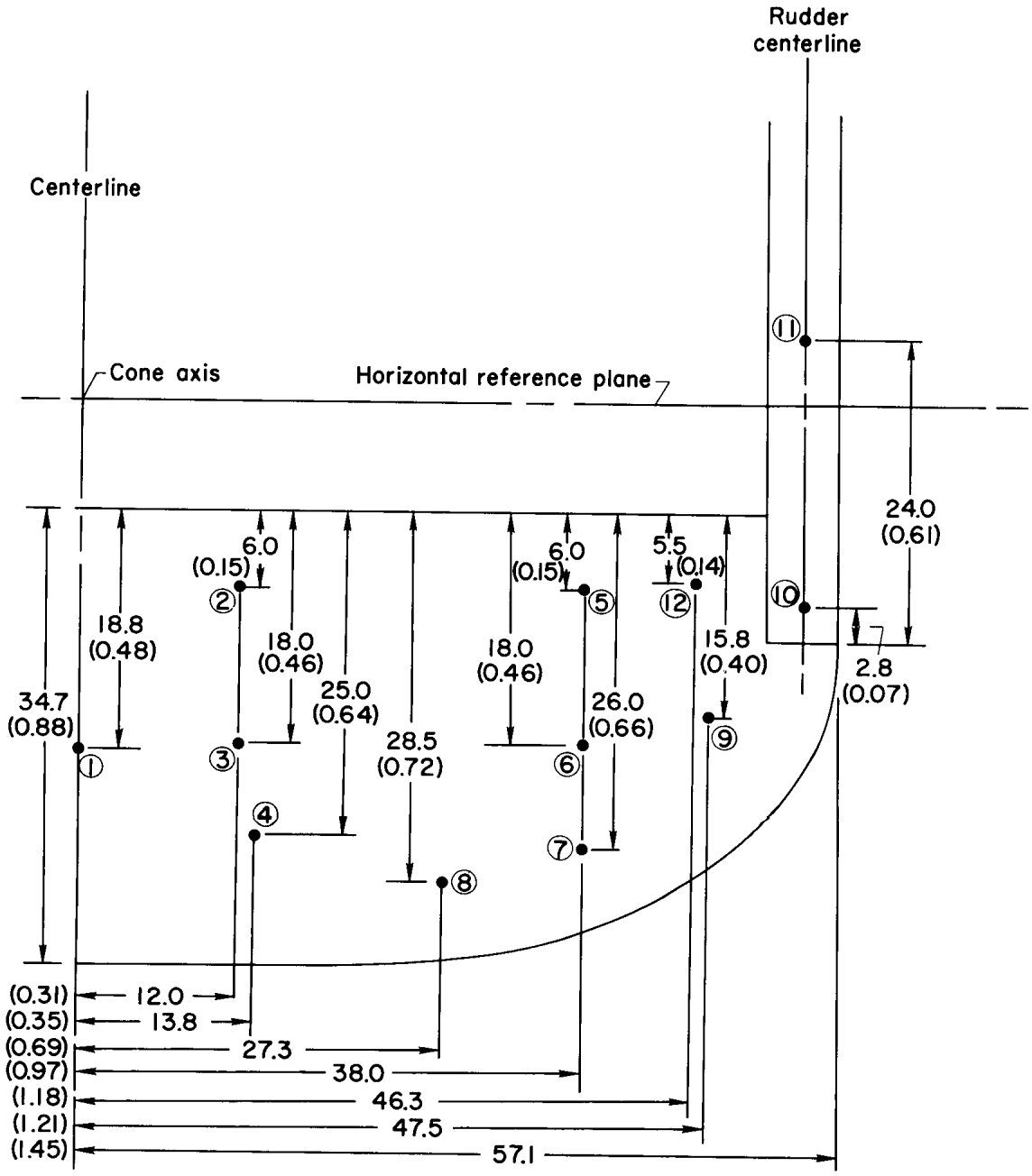

Figure 8.– Locations of base-pressure orifices. All dimensions in inches (meters).

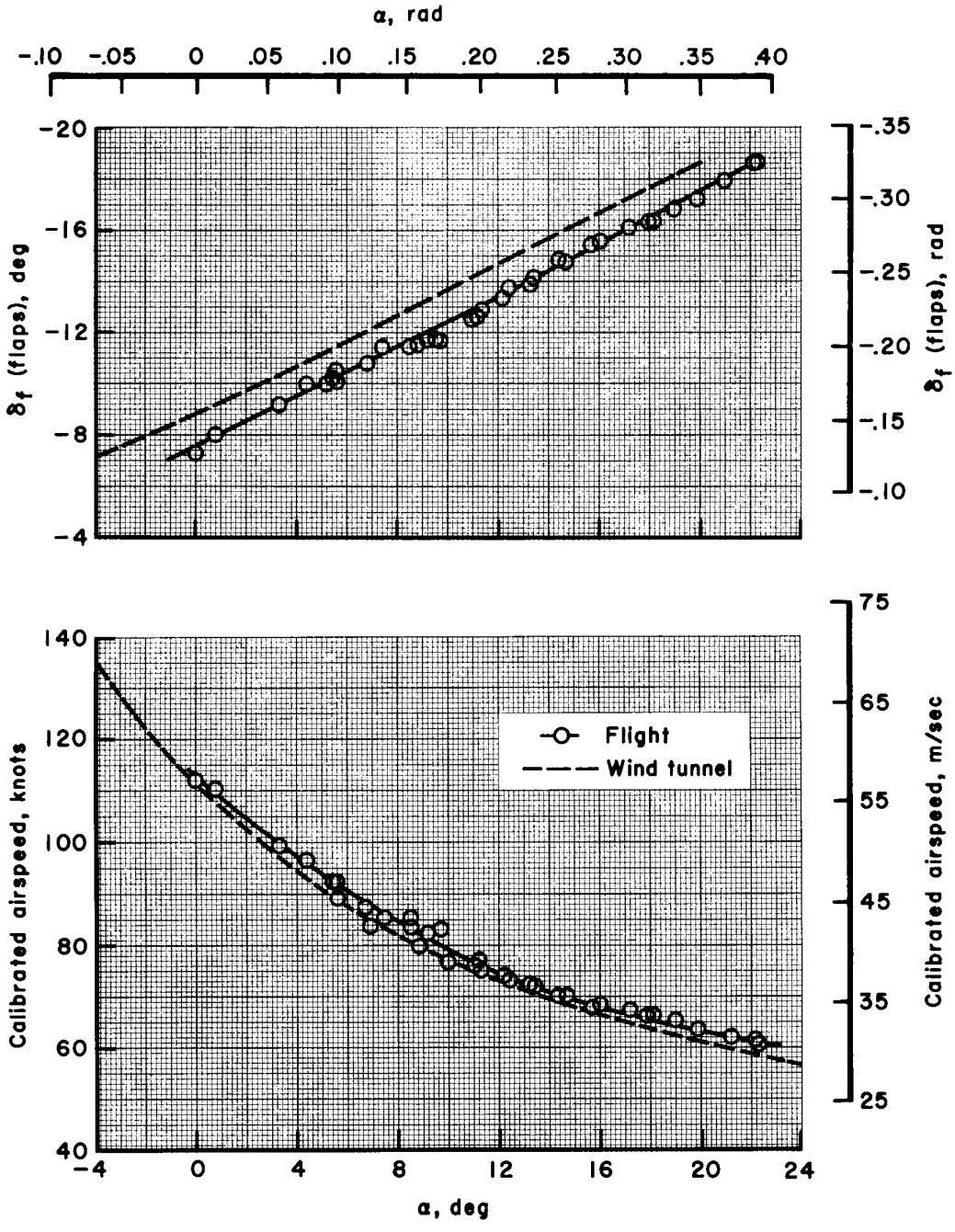

Figure 9.- Trim characteristics.

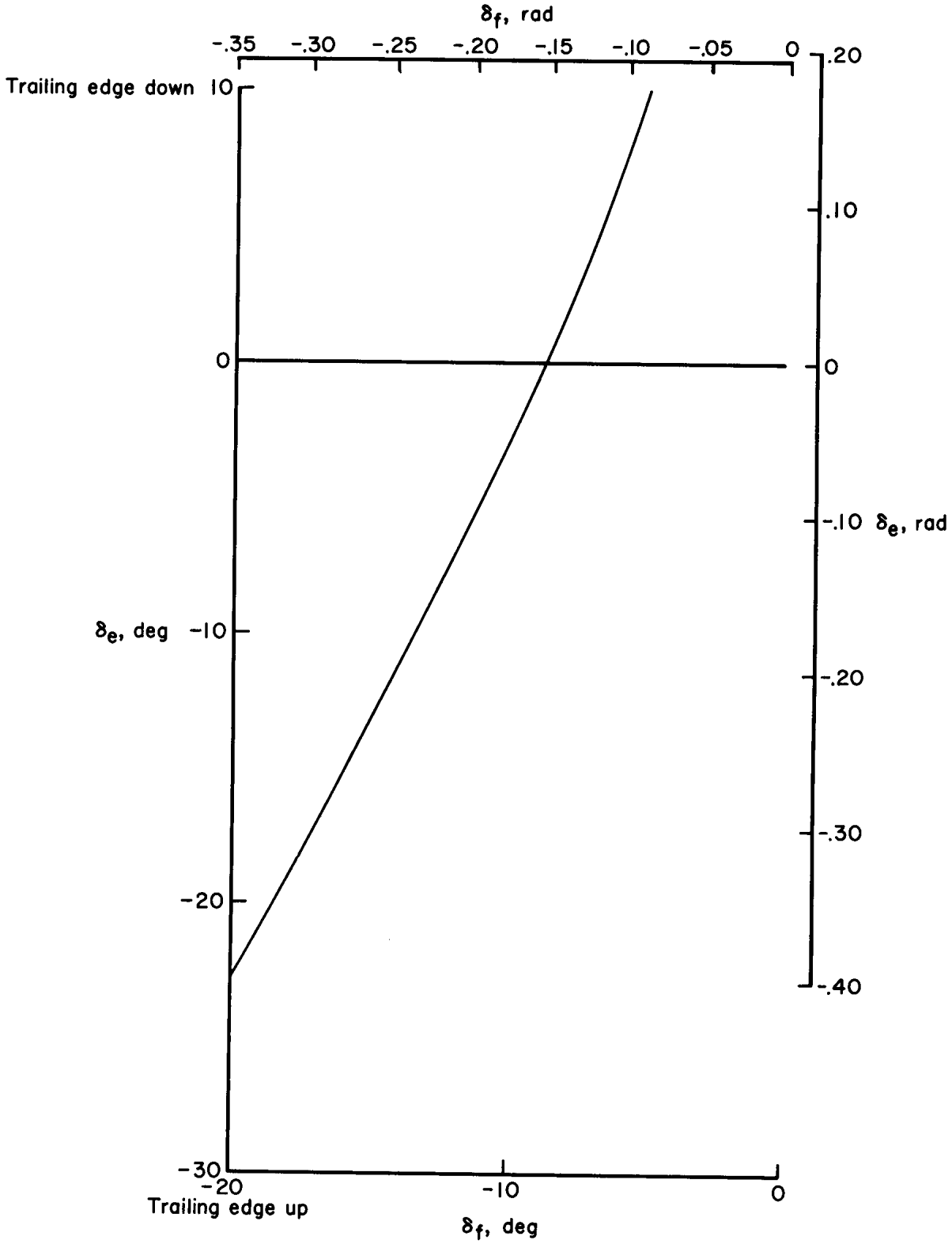

Figure 10.– Flap-elevon relationship for wind-tunnel tests, and as measured in the hangar.

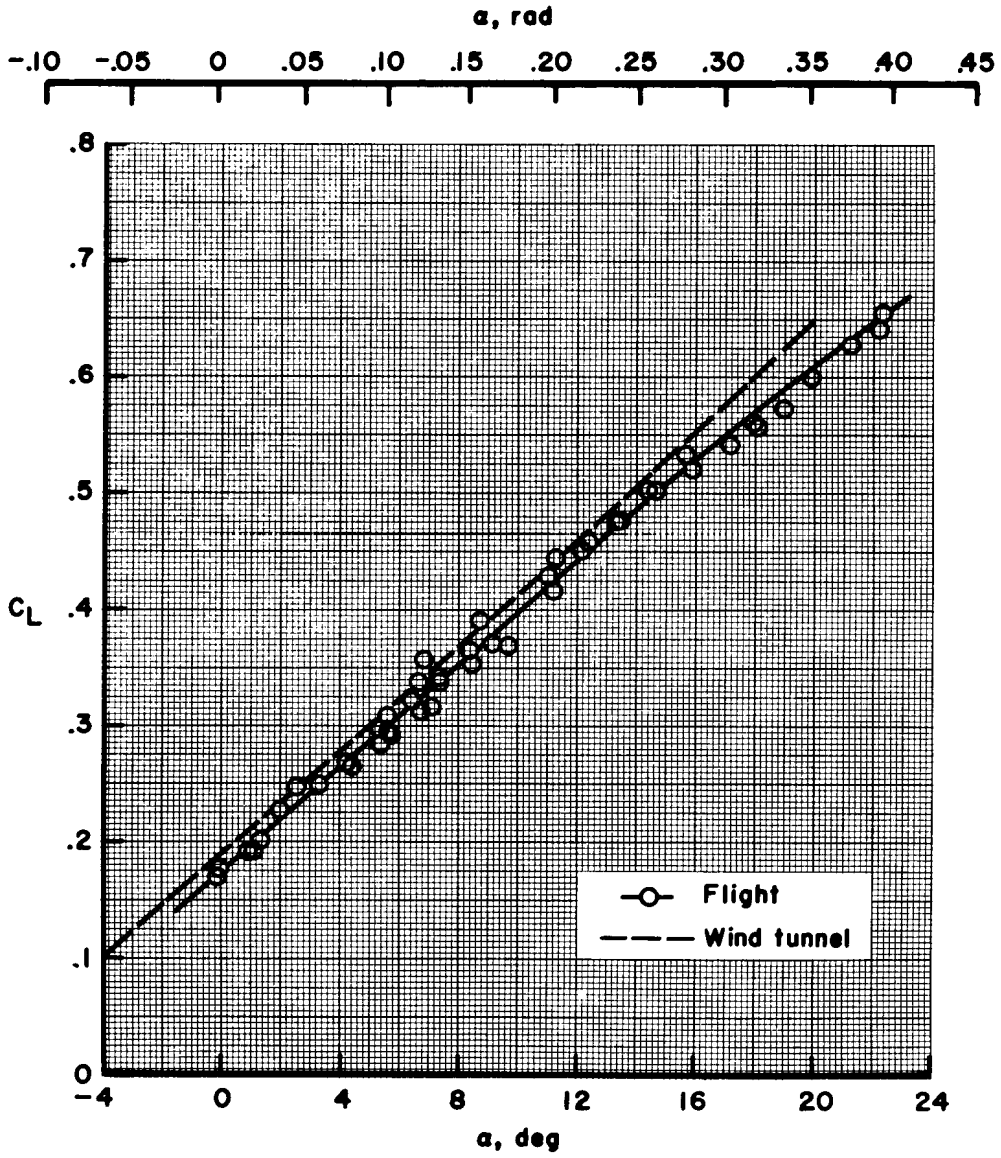

Figure 11.– Lift curve, trimmed.

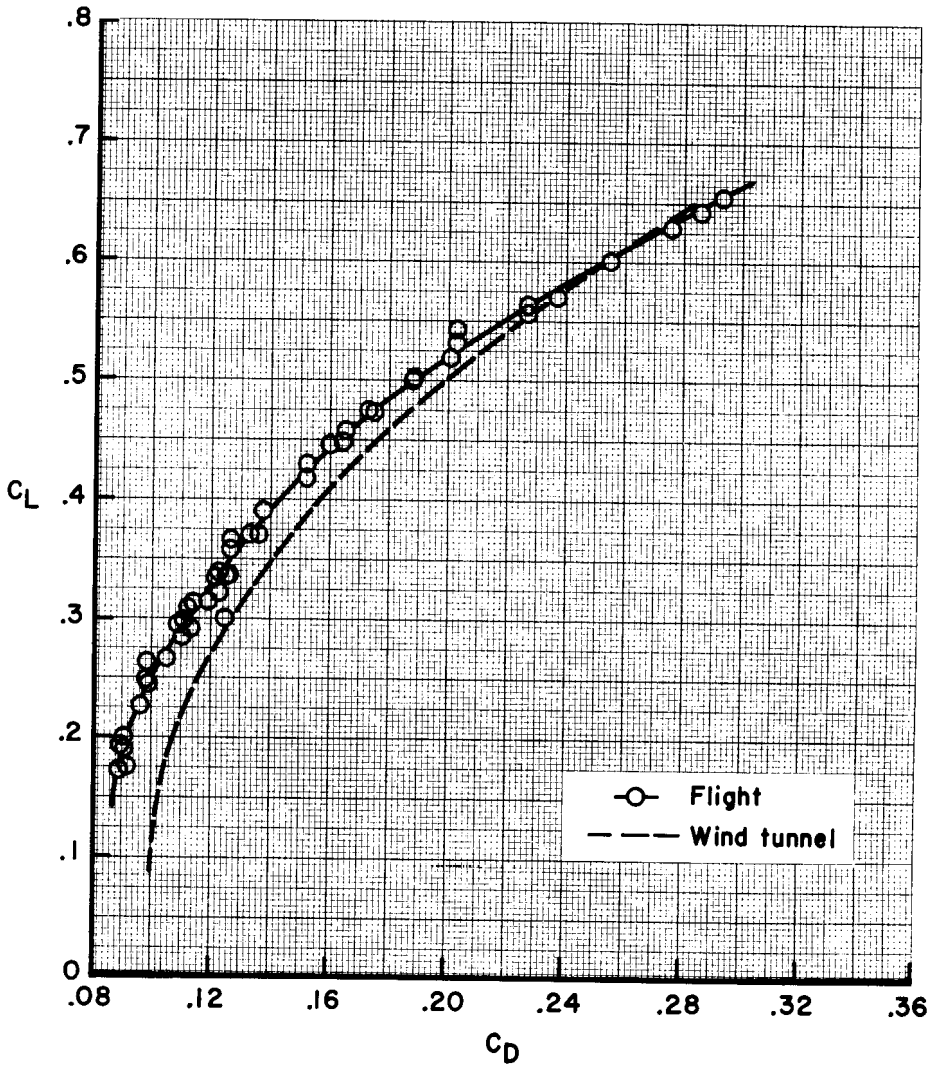

Figure 12.- Drag polars, trimmed.

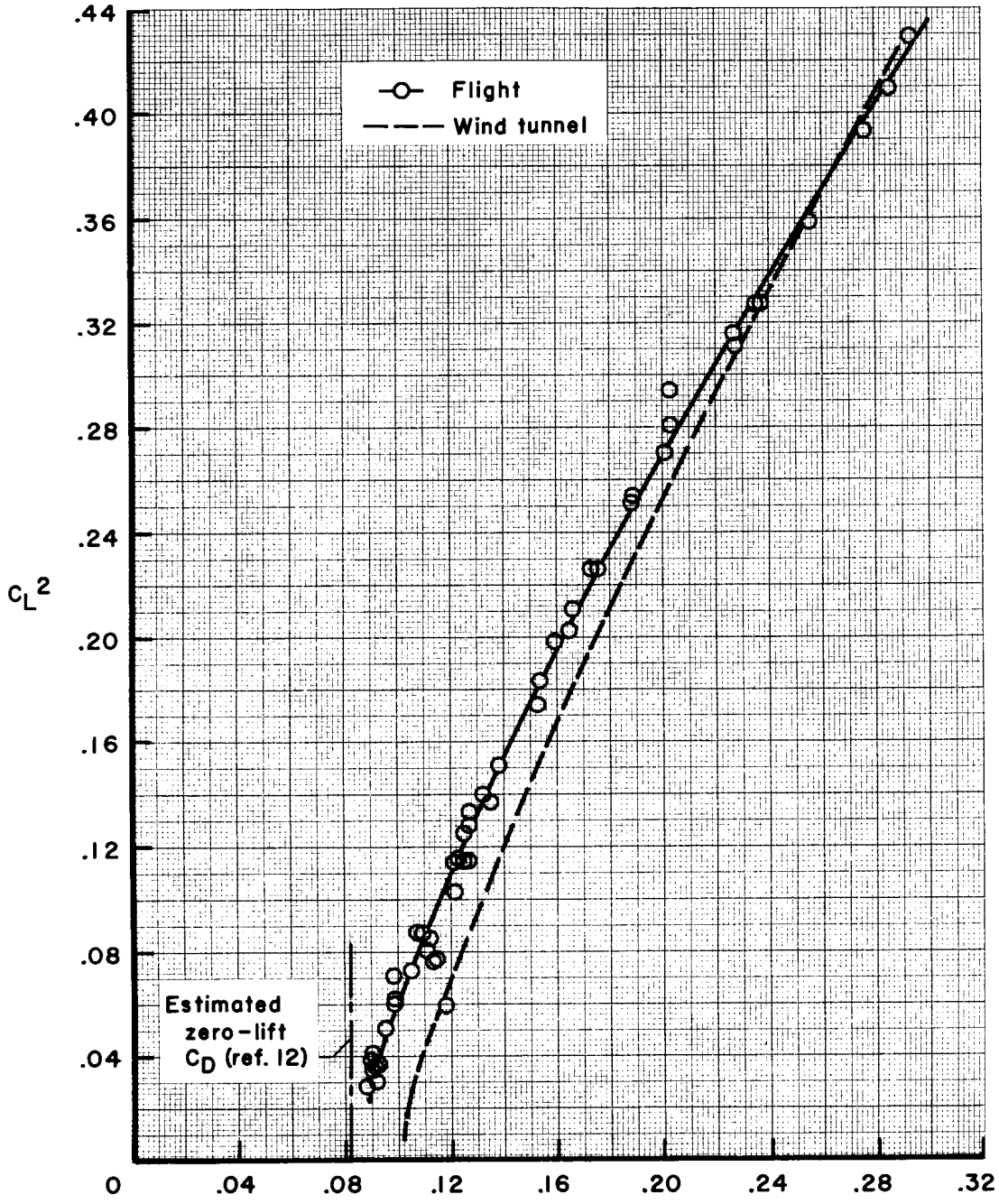

Figure 13.- Linearized form of the drag polar, trimmed.

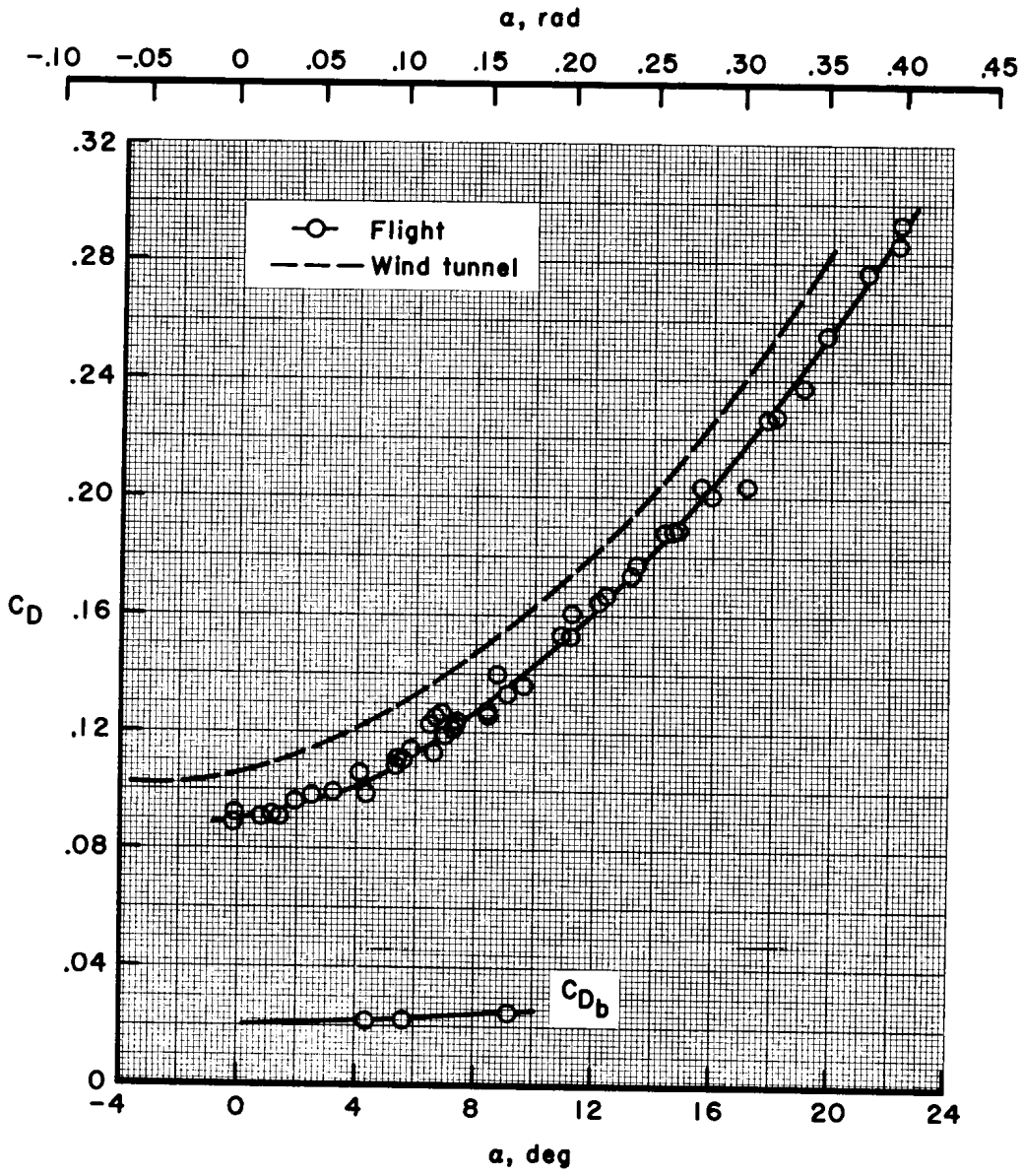

Figure 14.– Drag versus angle of attack, trimmed.

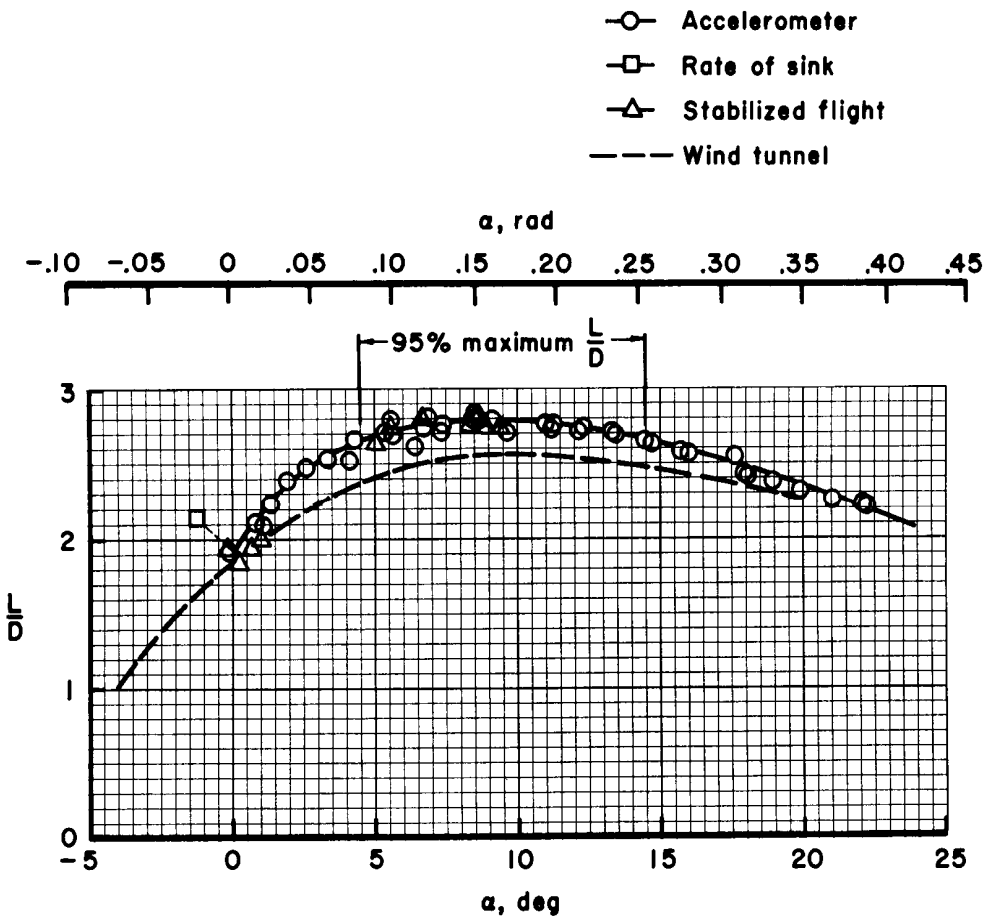

Figure 15.- Lift/drag ratio, trimmed.

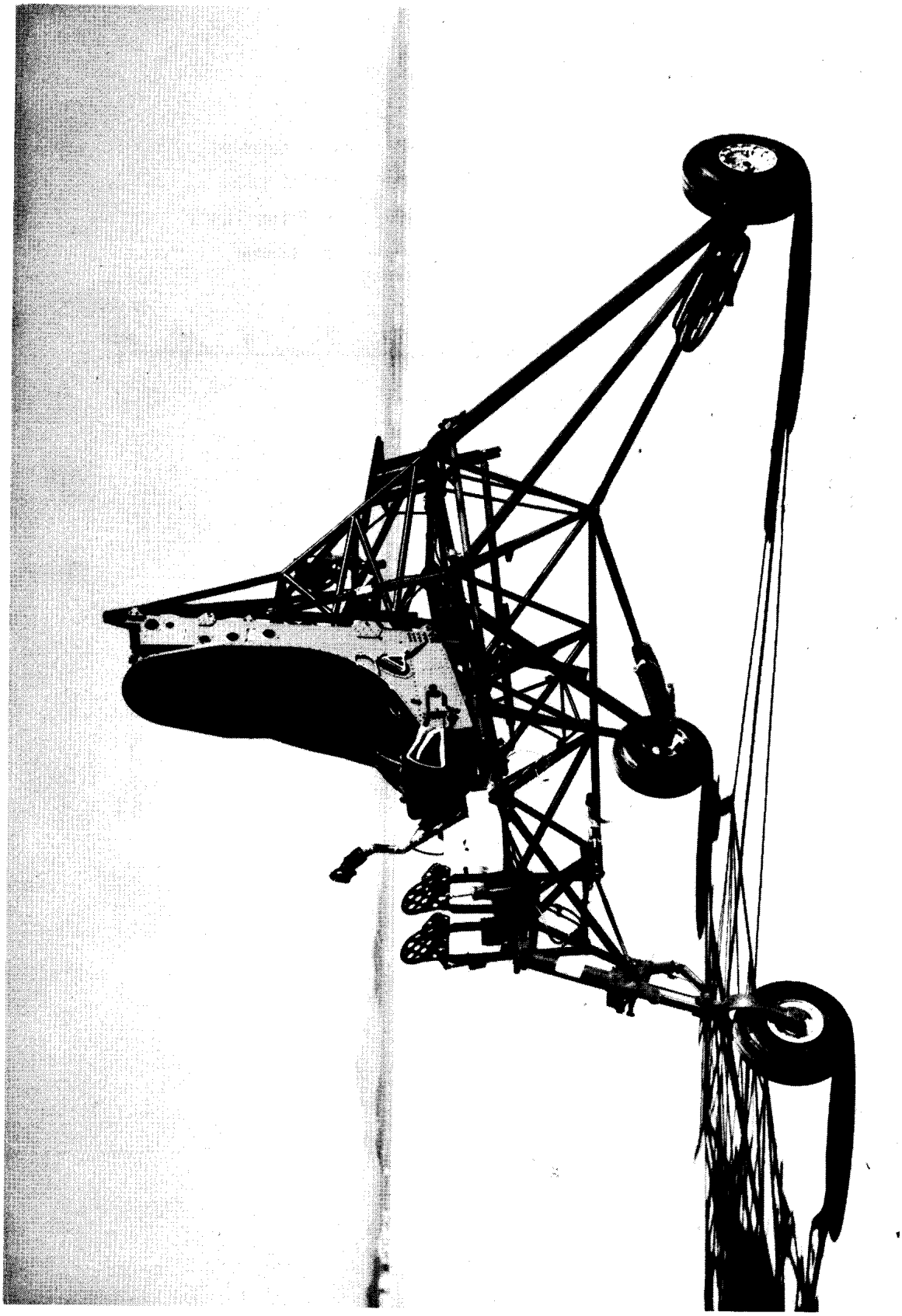

E-10756

Figure 16.- Internal structure of the M2-F1.

NASA-Langley, 1965 H-373